

Parametric wave interaction in quadratic crystal with randomized distribution of ferroelectric domains

K. Kalinowski^{1,2}, V. Roppo³, T. Łukasiewicz⁴, M. Świrkowicz⁴, Y. Sheng¹, and W. Krolikowski¹

¹ Laser Physics Center, Research School of Physics and Engineering, Australian National University, Canberra, ACT 0200, Australia, e-mail: xkk124@physics.anu.edu.au

² Nonlinear Physics Center, Research School of Physics and Engineering, Australian National University, Canberra, ACT 0200, Australia

³ Departament de Física i Enginyeria Nuclear, Escola Tècnica Superior d'Enginyeries Industrial y Aeronàutica de Terrassa, Universitat Politècnica de Catalunya, Colom 11, 08222 Terrassa, Barcelona, Spain

⁴ Institute of Electronic Materials Technology, Wólczyńska 133, 01-919 Warsaw, Poland

The date of receipt and acceptance will be inserted by the editor

Abstract We study the parametric wave interaction in quadratic nonlinear media with randomized distribution of the ferroelectric domains. In particular, we discuss properties of second and cascaded third harmonic generation. We derive analytical formulas describing emission properties of the second and third harmonics in the presence of domain disorder and show that the latter process is governed by the characteristics of the constituent processes, i.e. second harmonic generation and sum frequency mixing. We demonstrate the role of randomness on various second and third harmonic generation regimes such as Raman-Nath and Čerenkov nonlinear diffraction. We show that the randomness-induced incoherence in the wave interaction leads to deterioration of conversion efficiency and angular spreading of harmonic generated in the processes relying on transverse phase matching such as Raman-Nath. On the other hand forward and Čerenkov frequency generation are basically insensitive to the domain randomness.

1 Introduction

Periodic poling has been commonly used to realize efficient frequency conversion in ferroelectric crystals with quadratic nonlinearity [1]. The spatially periodic modulation of the sign of $\chi^{(2)}$ nonlinearity ensures the synchronization of the phases of interacting waves via the so called quasi phase matching [2,3,4]. In the simplest case of 1D periodically poled structure [Fig.1(a-b)] and collinear second harmonic generation the period of nonlinearity modulation Λ satisfies the following relation $|\mathbf{q}| = 2\pi/\Lambda = k_2 - 2k_1$. Here \mathbf{q} is the reciprocal vector of the nonlinearity modulation and k_1, k_2 are wave vectors of the fundamental and second harmonic, respectively. The quasi-phase matching technique is so versatile that by modulating spatially the domain pattern one can also spatially shape the wavefront of generated waves as has

been demonstrated in case of Bessel and Airy beams SHG [5, 6], however, because of resonant character of the quasi phase matching, perfectly periodic structure is efficient only for a particular choice of the wavelengths of interacting waves. Few methods have been proposed in order to extend the operational bandwidth of the QPM technique. They all rely on engineered poled structures and involve, for instance, structures consisting of periodically poled sections with different periods or multi-period and quasi-periodic structures, i.e. nonlinear superlattices [7,8,9,10,11]. Another possibility offer

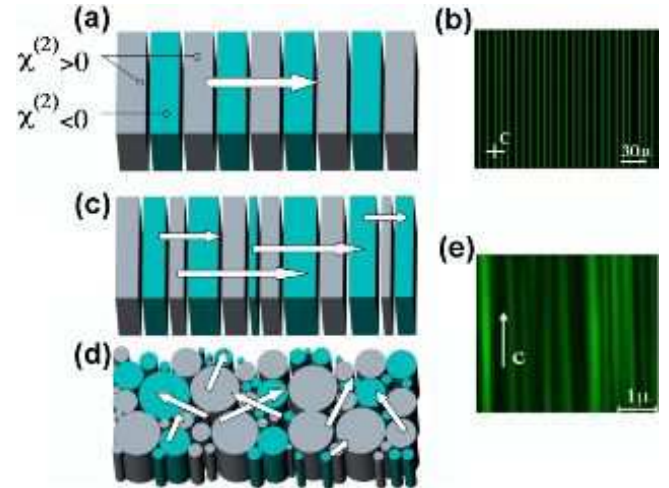


Fig. 1 (color online) (a) Illustrating the concept of periodically poled quadratic crystal. Arrow indicates the reciprocal grating vector. (b) Domain structure in commercial sample of periodically poled lithium niobate crystal with nominal poling period of $14\mu\text{m}$ (visualized via the second harmonic nonlinear microscopy). (c-d) Schematic representation of the quadratic crystal with (c) one- and (d) two-dimensional random spatial domain distribution. Arrows represent various reciprocal grating vectors. (e) Random ferroelectric domain pattern in SBN crystal (visualized via SH nonlinear microscopy [12]). 'C' in (b) and (e) indicates the direction of the optical C-axis.

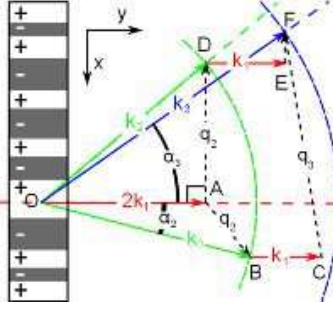


Fig. 2 (color online) Illustrating the phase matching conditions for the second and third harmonic generation via nonlinear diffraction in quadratic medium with randomized 1D ferroelectric domain structure. k_2 and k_3 represent wave vectors of the second and third harmonics, respectively. Green and blue rings (with corresponding radii k_2 and k_3) define all possible emission directions of the second and third harmonics.

media with random or randomized distribution of the sign of nonlinearity. In fact, Horowitz *et al.* [13] and Kawai *et al.* [14] were first to demonstrate broadband parametric interaction in unpoled strontium barium niobate (SBN) crystals. As-grown SBN crystals [Fig.1(d-e)] consist of elongated ferroelectric domains oriented along its optical (C) axis having random distribution of their size and orientation [15]. As such they represent disordered nonlinear medium. Such media have attracted a considerable attention in recent years due to their potential benefits for nonlinear parametric processes [16, 17, 18]. In the particular case of SBN crystal its spatially random distribution of nonlinearity [see Fig.1(d)] provides phase matching for second-order nonlinear processes for practically any incident wavelength [19] in its transmission band. The extensive studies of the second-order nonlinear processes in random SBN crystals resulted in demonstration of a number of effects including e.g., angular broadening of the emitted harmonics [20, 21], multi-frequency conversion [22, 23, 24], conical and planar frequency emission [25, 26, 27] and its application for optical autocorrelator [28, 29]. Few recent works have demonstrated beneficial effect of controlled randomization of originally periodic domain pattern on second harmonic generation [30, 31]. It should be also mentioned that the randomness of the ferroelectric domains pattern can be introduced inadvertently in the fabrication of QPM structures via periodic poling [see Fig.1(b)]. This typically has an adverse consequences on the intended performance of the QPM device leading, e.g. to decreased frequency conversion efficiency [4, 32, 33, 34, 35].

It has been also shown recently that under certain conditions the ferroelectric crystal with random domain distribution can be used for broadband cascaded third harmonic generation [19, 36, 37, 38, 39]. In such case the randomness of the nonlinearity contributes to both constituent processes: second harmonic and sum frequency generation. Subsequently, as the experiments showed, the spatial light intensity distribution of the emitted third and second harmonics are significantly different. So far, no theoretical analysis of the spatial proper-

ties of light emissions in the cascaded process has been conducted.

In this work we present extensive theoretical studies of the non-collinear second and third harmonic emission in ferroelectric crystal with randomized domain structure. Using the exact analytical formulas for the intensity of generated waves obtained in the regime of strong fundamental beam we compare the emission characteristics of both harmonics as a function of the degree of disorder and the wavelength.

2 Sum Frequency Mixing

Let us consider interaction of two optical waves with amplitudes E_a, E_b with the frequencies ω_a and ω_b in quadratic crystal with the spatially modulated sign of nonlinear coefficient $M(\mathbf{r})$. The nonlinearity will lead, among others, to the generation of the third wave E_{SF} at the frequency $\omega_{\text{SF}} = \omega_a + \omega_b$ whose amplitude can be expressed as [40]:

$$E_{\text{SF}}(\mathbf{q}) \propto idE_a E_b^* \int \int_A M(\mathbf{r}) e^{i\mathbf{q}\mathbf{r}} d\mathbf{r} \quad (1)$$

where d is the nonlinearity coefficient and integration is performed over the whole area A of the nonlinear crystal. Here $\mathbf{q} = \mathbf{k}_a - \mathbf{k}_b$ with $k_i = n_i 2\pi / \lambda_i$ representing wave vector and n_i is refractive index of the corresponding wave. In this paper we consider periodic structure with modulation only in x direction (Fig. 2) such that:

$$M(\mathbf{r}) = \sum_{j=0}^{N-1} (-1)^j \Pi_{x_j, x_{j+1}}(x) \quad (2)$$

where x_j is a position of j -th domain wall, N is number of domains and $\Pi_{x_j, x_{j+1}}(x) = 1$ for $x_j \leq x \leq x_{j+1}$ and 0 otherwise. In this case integral (1) can be separated into x and y directions. Additionally, because $M(\mathbf{r}) = 0$ outside crystal integration can be extended into infinity and one gets:

$$\begin{aligned} E_{\text{SF}}(\mathbf{q}) &\propto idE_a E_b^* \int_0^{L_y} e^{iq_y y} dy \int_0^{L_x} M(x) e^{iq_x x} dx \\ &\propto idE_a E_b^* L_y \text{sinc}\left(\frac{q_y L_y}{2}\right) M(q_x) \end{aligned} \quad (3)$$

where L_x, L_y are the lengths of the crystal in x, y directions and $M(q_x)$ denotes a Fourier transform of spatially modulated nonlinear coefficient:

$$M(q_x) = \frac{i}{q_x} \left(2 \sum_{j=1}^N (-1)^j e^{iq_x x_j} - (-1)^N e^{iq_x x_N} + 1 \right) \quad (4)$$

In general the last two terms in the bracket can be neglected [4] what results in:

$$M(q_x) = \frac{2i}{q_x} \sum_{j=1}^N (-1)^j \prod_{k=1}^j e^{iq_x x_k} \quad (5)$$

where $l_k = x_k - x_{k-1}$ is the width of k -th domain. If the domains' widths l_k are not equal but are subject to some random process then one has to take into account the statistical properties of this process. Additionally when generation results from many domains the intensity of generated wave $I_{\text{SF}} = |E_{\text{SF}}|^2$ is represented by an average over different realization ($\langle \cdot \rangle$ denotes averaging over domains width l):

$$\langle I_{\text{SF}} \rangle \propto d^2 L_y^2 I_a I_b \text{sinc}^2 \left(\frac{q_y L_y}{2} \right) \langle |M(q_x)|^2 \rangle. \quad (6)$$

The expression $\langle |M(q)|^2 \rangle$ has been discussed before [4,41]. We adopted here the approach as described by Le Grand *et al.* with some modifications that allow us to extend the results of SHG to SFM and subsequently to the cascaded THG.

If domains width varies randomly it can be described by an arbitrary Probability Density Function (PDF) $w(l)$ with characteristic function $\varphi(q) = \int w(l) \exp(iql) dl$ and for $|\varphi(q)| < 1$ and large number of domains ($N \gg 1$) one obtains:

$$\langle |M(q)|^2 \rangle = \frac{4N}{q^2} \left(1 - 2\text{Re} \left(\frac{\varphi(q)}{\varphi(q) + 1} \right) \right) = \frac{4N}{q^2} f(q) \quad (7)$$

what is exactly the formula derived by Le Grand *et al.* [41].

The effect of averaging and above discussed simplification on SH intensity is shown in the Fig. 3. This picture compares the square modulus of Fourier coefficients calculated for three different cases: the gray solid line depicts $|M(q)|^2$ with $M(q)$ calculated from Eq. (4), red dashed line shows value of $\langle |M(q)|^2 \rangle$ where $|M(q)|^2$ is calculated as for grey line and then averaged over 300 randomly generated samples, finally the dotted blue line shows $\langle |M(q)|^2 \rangle$ calculated according to simplified Eq. (7). One can see that results obtained with the simplified equation are consisted with numerically averaged SH intensity calculated using the full model for both very small (a) ($\sigma=0.05\mu\text{m}$) and large (b) dispersion ($\sigma=10\mu\text{m}$). All curves were calculated assuming number of domains to be $N=500$.

In order to calculate the averaged SF intensity $\langle I_{\text{SF}} \rangle$ one has to choose a function that describes statistical distribution of the domain widths. A natural choice would be Gaussian distribution. However Gaussian model is only applicable to rather small values of dispersions σ (in comparison to the average domain size l_m) because for dispersions comparable or bigger then l_m it results in negative values of domain width. The more appropriate choice is therefore the Gamma distribution which is defined for $l \in (0, \infty)$ with the PDF as

$$w(l) = \frac{l^{k-1} \theta^{-k} e^{-\frac{l}{\theta}}}{\Gamma(k)}, \quad (8)$$

where k and θ are the so called shape and scale parameters, respectively and Γ is gamma function. In this case the characteristic function is $\varphi(q) = (1 - iq\theta)^{-k}$. Maximum of the distribution, i.e. the most likely value (or mode) is $l_m = (k-1)\theta$ while standard deviation is $\sigma = \sqrt{k}\theta^2$. Gamma, unlike the Gaussian distribution, enables one to account for all possible dispersions regardless of the mode value.

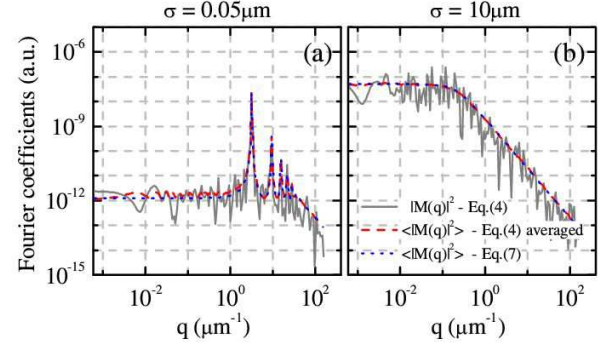


Fig. 3 (color online) Fourier coefficient of the sum frequency mixing process as a function of the phase mismatch parameter q for a periodic $\sigma=0.05\mu\text{m}$ (a) and randomized $\sigma=10\mu\text{m}$ (b) domain pattern. Solid (grey) and dashed (red) lines represent formula Eq.(4) calculated for particular realization of the domain distribution and averaged over 300 numerically generated random structures, respectively. Dotted (blue) line represents simplified formula (7) valid for large number of domain. The blue line almost exactly overlaps with the dashed red line.

In this paper, for the sake of clarity of the presented results, in all calculations we use Gamma distribution with fixed mode value $l_m = 1\mu\text{m}$ and we will characterize the randomness of the structure by its standard deviation σ .

3 Second Harmonic Generation

We consider the situation where the fundamental beam with the wavelength λ is incident onto the sample along the y direction (Fig. 2). Two photons of the fundamental harmonic $2k_1$, generate non-collinear SH with wave vector k_2 emitted at the angle α_2 such that the corresponding phase mismatch equals to $q_2 = k_2 - 2k_1$ (triangle OAB in Fig. 2). According to the formula Eq. (3) (with $E_a = E_b = E_1$) the amplitude of the generated SH electric E_2 field is given as

$$E_2(q_2) \propto idL_y I_1 \text{sinc} \left(\frac{q_2 L_y}{2} \right) M(q_2), \quad (9)$$

and the averaged SH intensity $\langle I_2 \rangle$:

$$\langle I_2 \rangle \propto d^2 I_1^2 L_y^2 \text{sinc}^2 \left(\frac{q_2 L_y}{2} \right) \langle |M(q_2)|^2 \rangle. \quad (10)$$

This formula relates the stochastic properties of the ferroelectric domain distribution to the spatial average intensity distribution of the SH. The most universal way to analyze this result is to use a 2D map plotting the Eq. (10) as a function of arbitrary phase mismatch components q_x and q_y . This is demonstrated in Fig. 4 where we show the average SH intensity ($\langle I_2 \rangle$) calculated for a sample with nominal domain width $l_m=1\mu\text{m}$ (what corresponds to poling period $\Lambda=2\mu\text{m}$) and four different values of dispersion σ : plots (a-d) correspond to the increasing degree of the randomness ranging

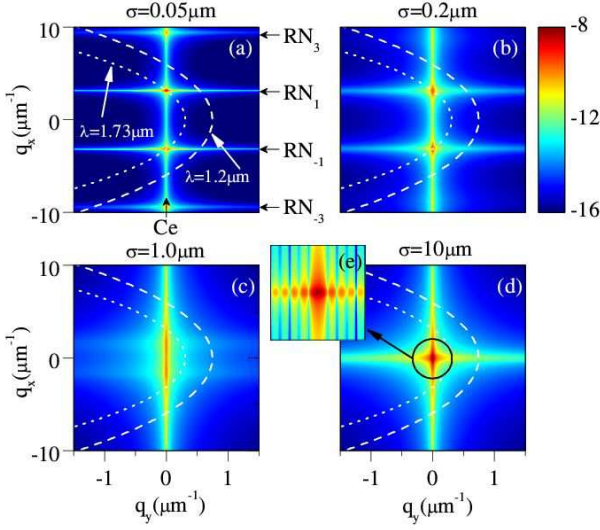


Fig. 4 (color online) Illustrating the effect of randomness on the strength of generation of the second harmonic in periodically poled media with random perturbation of the regular domain structure. Shown is the 2D map of the averaged intensity (in logarithmic scale) of the SH (Eq.10) as a function of the phase mismatch q_x and q_y . In all graphs the average domain size is $\bar{l} = 1\mu\text{m}$ while the dispersion of the domain size varies from $\sigma=0.05\mu\text{m}$ to $\sigma=10\mu\text{m}$. The dashed and dotted white curves represent all possible directions of the wave vectors of the second harmonics of the fundamental waves of $\lambda = 1.2\mu\text{m}$ and $\lambda = 1.73\mu\text{m}$, respectively. The inset depicts details of the map in the vicinity of $(q_x = 0, q_y = 0)$. Periodic oscillation of the intensity reflect the Makers fringes of the forward emission.

from $\sigma=0.05\mu\text{m}$ (almost ideal periodic structure), $\sigma=0.5\mu\text{m}$, $\sigma=1\mu\text{m}$ and $\sigma=10\mu\text{m}$ (strongly disordered structure). In case of periodic structure Fig. 4 (a) there are five characteristic lines/traces which correspond to the strong Fourier components of $M(q_x, q_y)$. These are: i) a vertical line at $q_y = 0$ which represents the Čerenkov SH radiation [42,43] (marked as Ce), ii) two symmetrically positioned horizontal lines at $q_x = \pm 3.1\mu\text{m}^{-1}$ corresponding to first order Raman-Nath resonance [44,45] (marked as $\text{RN}_{\pm 1}$), iii) two symmetrically positioned horizontal lines at $q_x = \pm 9.4\mu\text{m}^{-1}$ corresponding to the third order Raman-Nath resonances (marked as $\text{RN}_{\pm 3}$). When the dispersion of the domain size increases [(Fig. 4 (b))] the Raman-Nath emission lines shift towards the center and, at the same time, become broader and weaker until they disappear for strongly disordered structure (Fig. 4 (c-d)). On the other hand the Čerenkov SH signal can either increase or decrease depending on the value of q_x .

The dashed and dotted white curves represent phase mismatch (q_{2x}, q_{2y}) calculated for two arbitrary chosen wavelengths of the fundamental wave: $\lambda=1.2\mu\text{m}$ (dashed line), and $\lambda=1.73\mu\text{m}$ (dotted line) using reported refractive index of LiNbO_3 crystal [46]. If we fix fundamental beam wavelength (say, $\lambda=1.2\mu\text{m}$) it is clear that for almost periodic domain distribution the SH is efficiently generated only in those (q_x, q_y)

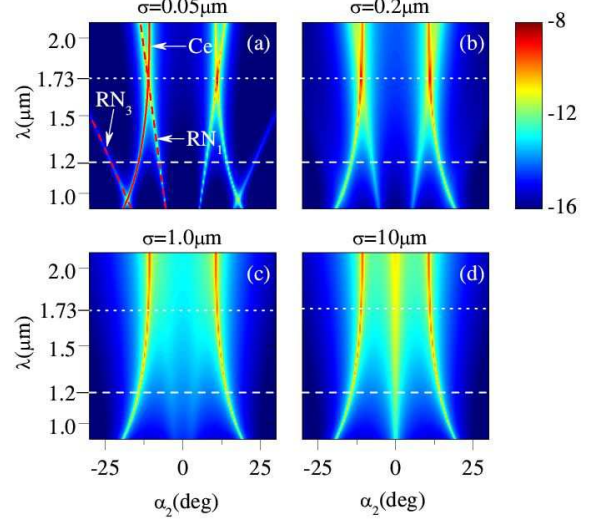


Fig. 5 (color online) Normalized intensity of the SH signal as a function of emission angle α_2 and wavelength of the fundamental beam λ for various degree of disorder: (a) $\sigma=0.05\mu\text{m}$, (b) $\sigma=0.2\mu\text{m}$, (c) $\sigma=1\mu\text{m}$ and (d) $\sigma=10\mu\text{m}$.

points where the phase mismatch curve intersects the lines corresponding to large value of the Fourier spectrum of the nonlinearity modulation. Those characteristic points result in a wavelength dependent spatial emission pattern of SH.

Fig. 5 shows the intensity of the SH (Eq. (10)) as a function of fundamental wavelength and SH emission angle α_2 . For a periodic structure [Fig. 5(a)] SH intensity exhibits clear peaks where the emission angles α_2 are defined by partial or full phase matching conditions. For Čerenkov SH emission, where $q_{2y} = 0$, the emission angle can be calculated as:

$$\cos(\alpha_2^{Ce}) = \frac{n_1}{n_2}, \quad (11)$$

and for m -th order Raman-Nath where $q_{2x} = m2\pi/\Lambda$, emission angle is:

$$\sin(\alpha_2^{RN_m}) = m \frac{\lambda}{2\Lambda n_2}. \quad (12)$$

Those wavelength dependent emission angles are plotted in the Fig.5 (a) as a red solid line (marked as Ce) for α_2^{Ce} and as red dashed lines (marked as RN_1, RN_3) for $\alpha_2^{RN_m}$. As it has been mentioned earlier, it is clearly seen that the emitted Raman-Nath SH exhibits enhanced angular spreading for strong domain dispersion while Čerenkov emissions is less sensitive to disorder.

The horizontal dashed and dotted lines in Fig. 5 point to two arbitrary chosen wavelengths of the fundamental beam $\lambda=1.2\mu\text{m}$ (white dashed line) and $\lambda=1.73\mu\text{m}$ (white dotted line). The corresponding second harmonic angular intensity profiles for $\sigma=0.05\mu\text{m}$ (red solid lines) and $\sigma=10\mu\text{m}$ (blue dashed line) are depicted in Fig.6. The strong modification of the emission pattern with high degree of randomness is evident, however it affects SH in different ways depending

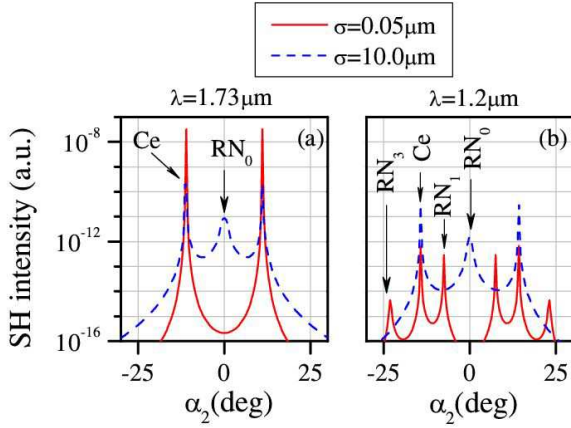


Fig. 6 (color online) SH intensity as a function of the emission angle α_2 for $\sigma=0.05\mu\text{m}$ (cross section along dotted line in Fig. 5(a)) and $\sigma=10\mu\text{m}$ (cross-section along dotted line in Fig. 5(d)). Fundamental wavelength $\lambda=1.73\mu\text{m}$ (a) and $\lambda=1.2\mu\text{m}$ (b).

on the wavelength and the type of interaction. For $\lambda=1.73\mu\text{m}$ [Fig.6(a)] we can see that increasing of σ suppresses intensity of the Čerenkov (Ce) signal. On the other hand for $\lambda=1.2\mu\text{m}$ [Fig.6(b)] Ce emission significantly increases while first and third order Raman-Nath peaks (RN_1 and RN_3) practically vanish. For both wavelengths strong dispersion produces zero order Raman-Nath (RN_0) reciprocal vectors.

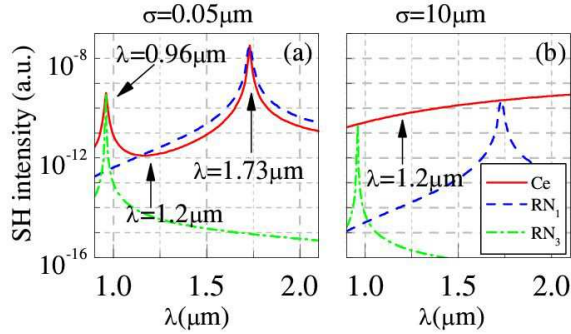


Fig. 7 (color online) Intensity of the Čerenkov and Raman-Nath second harmonic signals as a function of fundamental wavelength for different dispersions of the domain size: (a) $\sigma=0.05\mu\text{m}$ and (b) $\sigma=10\mu\text{m}$. Red solid line (Ce) represents Čerenkov intensity, blue dashed line (RN_1) is the first order Raman-Nath and the green dashed-dotted line (RN_3) represents the third order Raman-Nath.

Fig. 7 shows Čerenkov SH (red solid line), Raman-Nath first (blue dashed line) and third order (green dashed-dotted line) SH as a function of wavelength for two different dispersions $\sigma=0.05\mu\text{m}$ [Fig 7(a)] and $\sigma=10\mu\text{m}$ [Fig. 7(b)]. Those plots can be also understood as profiles along vertical red curves marked on a the Fig. 5(a) as Ce, RN_1 and RN_3 respectively. One can notice that Čerenkov radiation (Ce) is a

subject to intensity modulation. The most efficient SH emission is expected where the Raman-Nath and Čerenkov signals overlap (as it happens for $\lambda=1.73\mu\text{m}$ and $\lambda=0.96\mu\text{m}$) what constitutes the regime of so called nonlinear Bragg diffraction [47], i.e. SH emission under simultaneous fulfillment of the transverse and longitudinal phase matching. For strong disorder the peak intensity deteriorates due to decrease in RN intensity. However at some wavelengths (as for $\lambda=1.2\mu\text{m}$) the Ce intensity increases. This strong dependence of the Čerenkov signal on the wavelength is a result of the interference of many SH components emitted by each ferroelectric domain [48]. When the initially periodic domain pattern becomes disordered the interference effect gets weaker and the total Čerenkov signal is determined by the sum of the intensities of contributing waves. In effect, the Čerenkov signal which was strong for certain fundamental wavelength (due to a constructive interference) is weakened while the one which was initially weak (due to destructive interference) increases.

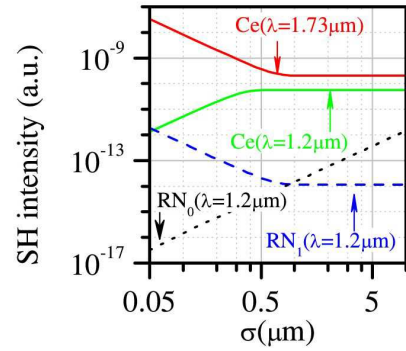


Fig. 8 (color online) Intensity of the Čerenkov (Ce), zero (RN_0) and first (RN_1) order Raman-Nath signals as a function of the domain dispersion σ , for $\lambda = 1.2\mu\text{m}$ and $\lambda = 1.73\mu\text{m}$ (as depicted in brackets).

This is even clearer in the Fig. 8 where we plot the Čerenkov, zero and first order Raman-Nath as a function of domain dispersion σ . We can see that with growing disorder Raman-Nath $RN_1(\lambda=1.2\mu\text{m})$ and Čerenkov $Ce(\lambda=1.73\mu\text{m})$ signals decrease and tends to a constant value as the constructive interference effects associated with periodicity of the domain distribution are no longer relevant for large σ . On the other hand signal $Ce(\lambda=1.2\mu\text{m})$ increases due to weakening of destructive interference effect. Zero order Raman-Nath $RN_0(\lambda=1.73\mu\text{m})$, initially not present for perfect structure i.e. $\sigma \rightarrow 0$, continuously increases with σ as the high degree of disorder provides small but nonzero fourier coefficients for $q_{2x}=0$ which, in case of SH, contribute towards the forward emission.

4 Third Harmonic Generation

It has been demonstrated recently that nonlinear crystals with random domain distribution enable third harmonic generation via cascading of the frequency doubling and sum fre-

quency mixing [19,36,38,39]. In this section we provide the first analytical study of such process by extending the approach discussed in the previous two sections. We will consider the same setting of the one-dimensional sample of the quadratic crystal with randomized domain distribution being illuminated by the strong fundamental beam. The nonlinear interaction leads to simultaneous emission of the second and third harmonics. To calculate the amplitude of the third harmonic we use Eq.(3) where $E_a = E_2$ is taken from Eq.(9) and $E_b = E_1$. In this case the amplitude of the electric field of the third harmonic E_3 is

$$E_3(\mathbf{q}_2, \mathbf{q}_3) \propto -d^2 L_y^2 E_1^* I_1 \text{sinc}\left(\frac{q_{2y} L_y}{2}\right) \text{sinc}\left(\frac{q_{3y} L_y}{2}\right) \times M(q_{2x}) M(q_{3x}) \quad (13)$$

where \mathbf{q}_2 and \mathbf{q}_3 represent the phase mismatch of the first and the second process of sum frequency mixing, respectively. The phase matching diagram of the TH generation via cascading process is illustrated in Fig. 2. This graph represents relevant processes in this multi-wave interaction. First a photon of SH is generated in the frequency doubling process with the phase mismatch wave vector of q_2 and emitted at the angle α_2 as depicted by the triangle OAB. Then this photon together with photon of the fundamental wave (BC) forms a photon (OF) with the triple frequency of the fundamental where TH and phase mismatch vector $\mathbf{q}_3 = \mathbf{k}_3 - \mathbf{k}_2 - \mathbf{k}_1$. The TH wave is emitted in the direction determined by the angle α_3 (angle between OF and OA). In order to reveal key features of this cascaded process we will first calculate the average intensity of the TH wave $I_3 = \langle |E_3|^2 \rangle$ generated in such a single process:

$$\langle I_3 \rangle \propto d^4 L_y^4 I_1^3 \text{sinc}^2\left(\frac{q_{2y} L_y}{2}\right) \text{sinc}^2\left(\frac{q_{3y} L_y}{2}\right) \times \langle |M(q_{2x})|^2 |M(q_{3x})|^2 \rangle \quad (14)$$

where:

$$\langle |M(q_{2x})|^2 |M(q_{3x})|^2 \rangle = \frac{16}{q_{2x}^2 q_{3x}^2} \times (N^2 f(q_{2x}) f(q_{3x}) + N O_1 + O_2), \quad (15)$$

where O_1 , O_2 are function of phase mismatch q_{2x} , q_{3x} and characteristic function $\varphi(q)$ and where $M(q_x)$ was taken from Eq. (5). When $N \gg 1$ and $|\varphi(q)| < 1$ terms containing O_1 and O_2 can be neglected and above simplifies to:

$$\langle I_3 \rangle \propto 16 d^4 L_y^4 I_1^3 N^2 \text{sinc}^2\left(\frac{q_{2y} L_y}{2}\right) \text{sinc}^2\left(\frac{q_{3y} L_y}{2}\right) \times \frac{f(q_{2x}) f(q_{3x})}{(q_{2x})^2 (q_{3x})^2} = \frac{1}{I_1} \cdot \langle I_{\text{SF}}(\mathbf{q}_2) \rangle \langle I_{\text{SF}}(\mathbf{q}_3) \rangle. \quad (16)$$

The above equation shows that the resulting intensity of the third harmonic is a product of intensities of two constituent sum frequency mixing processes where both processes utilize the same Fourier space.

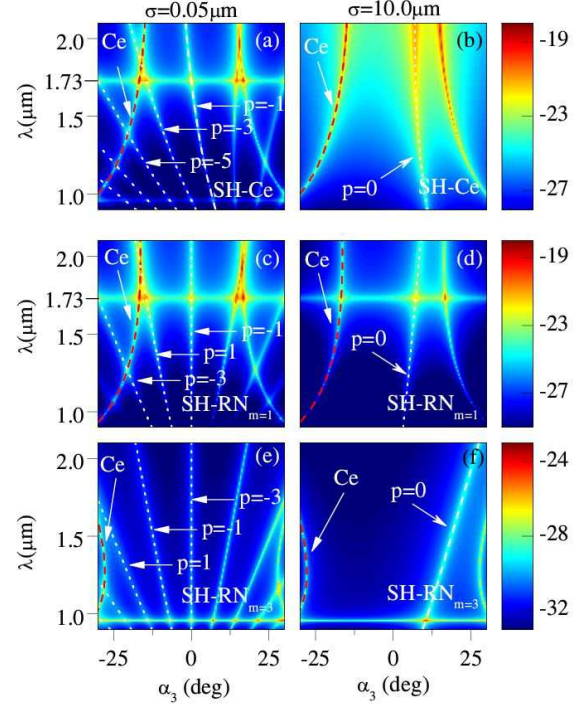


Fig. 9 (color online) Normalized intensity of the TH signal as a function of the wavelength of the fundamental beam and emission angle for very weak ($\sigma=0.05\mu\text{m}$ - left column) and strong ($\sigma=10\mu\text{m}$ - right column) domain dispersion. Pairs of graphs (a,b), (c-d) and (e-f) correspond to three distinct interaction mechanisms representing different type of the SH emission according to Eq. (16). They include the cases of second harmonic emitted as a Čerenkov (a,b), as well as first (c-d) and third (e-f) order Raman-Nath waves.

Since TH is generated in a cascaded process and its strength depends on the strength of the SH generated in a first step it is natural to analyze how SH generated in different processes like Čerenkov or Raman-Nath affects spatial TH emission. Fig. 9(a) show TH intensity $\langle I_3 \rangle$ calculated according to Eq. (16) as a function of the fundamental wavelength and TH emission angle α_3 resulting only from SH generated in a Čerenkov-like process, i.e. fixed values of SH phase mismatch vector to $q_{2y} = 0$ and $q_{2x} = q_2 \sin(\alpha_2^{Ce})$. One can clearly observe a number of curves of enhanced TH intensity. Periodic structure exhibits strong resonances in Fourier space [see Fig.4(a)] and since both processes, SHG and following SFM utilize the same Fourier space it is expected to obtain high TH intensities for processes resulting from either Čerenkov or Raman-Nath resonances [45]. The emission angle α_3 of TH generated in double Čerenkov process (ie when $q_{3y} = 0$) can be calculated as:

$$\cos(\alpha_3^{Ce+Ce}) = \frac{n_1}{n_3} \quad (17)$$

Angle α_3^{Ce+Ce} as a function of wavelength λ is plotted in Fig. 9(a) as a dashed red line (marked as Ce) and it exactly overlaps with one of the TH signals. Similarly the remaining traces can

be identified as interaction of Second Harmonic Čerenkov with following Sum Frequency Mixing of p -th order Raman-Nath (ie. $q_{3x} = p2\pi/\Lambda$) where the emission angle α_3 is:

$$\sin(\alpha_3^{\text{Ce}+\text{RN}_p}) = \frac{2\Lambda\sqrt{n_2^2 - n_1^2} + \lambda p}{3\Lambda n_3} \quad (18)$$

For the sake of clarity we plotted only few traces: RN_{-1} , RN_{-3} and RN_{-5} . The strong horizontal line at $\lambda=1.73\mu\text{m}$ and the weaker one at $\lambda=0.96\mu\text{m}$ result from the strong SH generation at this wavelengths due to Čerenkov resonance with RN_1 and RN_3 as shown in Fig. 7.

When the domain structure becomes strongly disordered [Fig.9(b)] all the previously observed Raman-Nath peaks disappear. However, as in the case of SH also now the Čerenkov emission (red dashed line) remains relatively strong and additionally the zero order Raman-Nath (RN_0) is present (white dotted line).

Analogously Figs. 9(c,d) show average intensity of the third harmonic ($\langle I_3 \rangle$) but this time SH is generated as a first order Raman-Nath ($m = 1$) and Figs. 9(e-f) third order ($m = 3$) Raman-Nath. The formulas for emission angles in those processes are:

$$\cos(\alpha_3^{\text{RN}_m+\text{Ce}}) = \frac{n_1 \pm n_2 \sqrt{4 - m^2 \frac{\lambda^2}{\Lambda^2 n_2^2}}}{3n_3} \quad (19)$$

for TH generated as a Čerenkov (red dashed line) or

$$\cos(\alpha_3^{\text{RN}_m+\text{RN}_p}) = \frac{\lambda(m+p)}{3\Lambda n_3} \quad (20)$$

when TH is generated as the p -th order Raman-Nath (indicated by white dotted line).

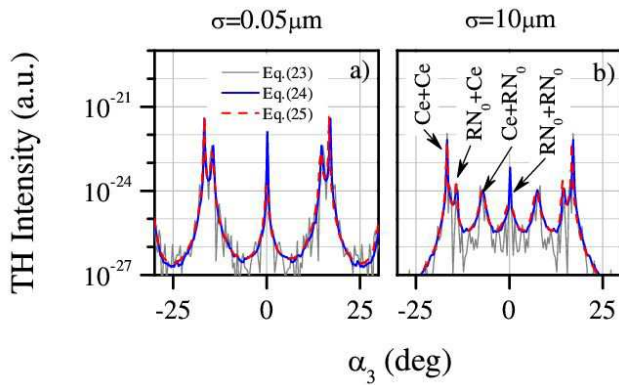


Fig. 10 (color online) Comparison of THG via coherent process according to Eq.(21) (gray lines) and incoherent Eq.(23) (red lines) for a) small dispersion $\sigma=0.05\mu\text{m}$ and b) large dispersion $\sigma=10\mu\text{m}$. The solid blue line represents coherent contributions to the overall THG averaged over an ensemble of 120 randomly generated realizations of domain pattern [Eq. 22]. Incident wavelength $\lambda=1.73\mu\text{m}$.

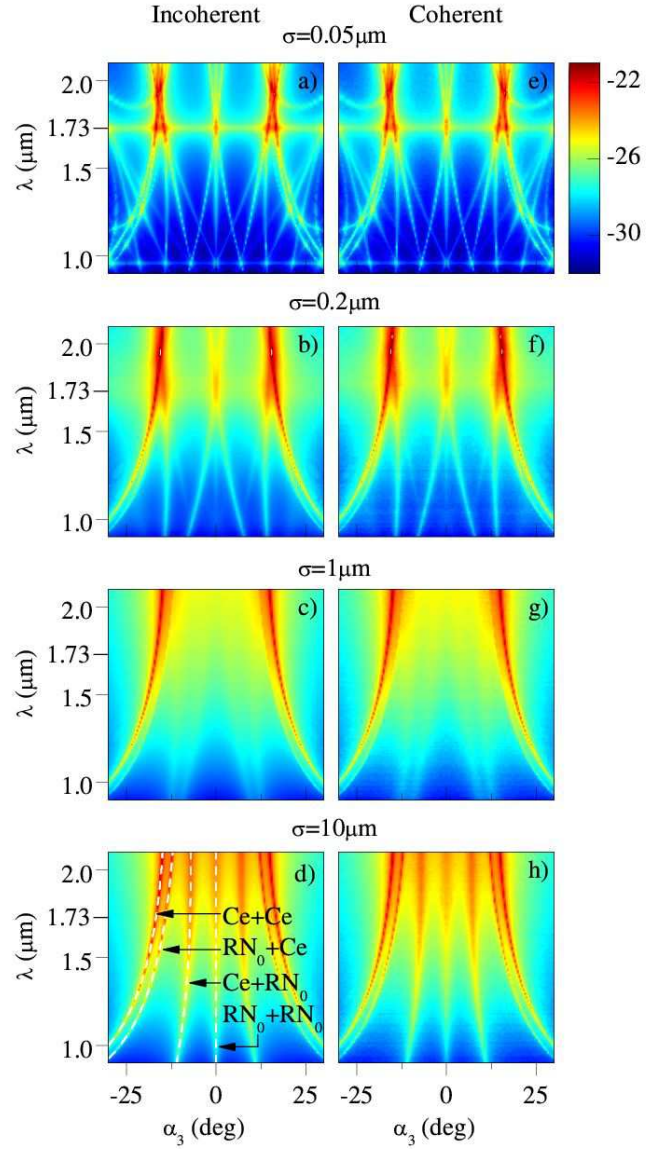


Fig. 11 (color online) Normalized intensity of the third harmonic as a function of the fundamental wavelength and emission angle in the regime of almost periodic ($\sigma=0.05\mu\text{m}$) and disordered ($\sigma=10\mu\text{m}$) ferroelectric domain distribution. Plots (a-d) in the left column are obtained assuming incoherent contribution to the total TH intensity according to Eq. 23. Plots shown in the right column are obtained by assuming coherent model Eq. 22, and by averaging the calculated TH intensity pattern over 45 different realizations of the domain distribution.

In experimental reality there is no possibility to limit THG to only selected processes and so in general the total intensity of the third harmonic I_3 would be a sum of TH generated from all possible emitted second harmonics. As described previously TH can be generated in a process OBCF as schematically shown in Fig.2. However, the TH with exactly the same wave vector can be also generated in an another process as for example the one indicated by ODEF in the same

figure. In order to calculate total TH emitted in a particular direction α_3 an integral over all possible SH emission angles α_2 has to be calculated:

$$I_3^{\text{coh}} = \left| \int E_3(\mathbf{q}_2, \mathbf{q}_3) d\alpha_2 \right|^2 \quad (21)$$

and in case of presence of randomness its averaged version is given as

$$\begin{aligned} \langle I_3^{\text{coh}} \rangle &\propto d^4 L_y^4 I_1^3 \left\langle \left| \int_{-\pi}^{\pi} \text{sinc} \left(\frac{q_{2y} L_y}{2} \right) \text{sinc} \left(\frac{q_{3y} L_y}{2} \right) \right. \right. \\ &\quad \left. \left. \times M(q_{2x}) M(q_{3x}) d\alpha_2 \right|^2 \right\rangle \end{aligned} \quad (22)$$

where averaging again is performed over all realizations of domains widths. Both integrals Eq. (21) and Eq. (22) cannot be simplified and can be evaluated only numerically. However our previous experiments in Third Harmonic Generation in nonlinear crystals with 3-dimensional fully random domain structure indicate that the emission process is in fact incoherent, i.e. the intensity of the TH is given as a superposition of intensities generated by all constituent second harmonic waves [36,38]. Therefore for large dispersion of domain sizes it is justified to calculate TH signal assuming incoherent emission

$$\langle I_3^{\text{inc}} \rangle = \int_{-\pi}^{\pi} \langle I_3 \rangle d\alpha_2 \propto \int_{-\pi}^{\pi} \langle I_{\text{sf}}(\mathbf{q}_2) \rangle \langle I_{\text{sf}}(\mathbf{q}_3) \rangle d\alpha_2 \quad (23)$$

where we use $\langle I_3 \rangle$ from Eq. (16).

In Fig.10 we show angular intensity profile of the third harmonic in case of two domain dispersions: $\sigma=0.05\mu\text{m}$ (a) and $\sigma=10\mu\text{m}$ (b) for fundamental wavelength $\lambda=1.73\mu\text{m}$. The grey noisy line represents the TH intensity based on coherent superposition of contributing second harmonic waves, calculated for a single particular realization of domain distribution (Eq. (21) with TH electric field E_3 taken from Eq.(13)). The solid blue line depicts coherently calculated intensity (same as grey line) but averaged over 120 realizations of randomly generated structures [Eq. (22)]. Finally, the dashed red line shows the intensity profile obtained by assuming an incoherent interaction according to Eq.(23). Both models clearly coincide confirming the incoherent character of third harmonic generation in that case. The labels next to the emission peaks in graph Fig.10 identify processes responsible for particular emission angle. The labeling convention used here and in Fig. 11 is such that the first symbol refers to the second harmonic process while the second to the sum frequency mixing. Notice how the high degree of randomness leads to increase of the forward emission of TH. This is a direct consequence of the disorder-enhanced forward emission of the second harmonic as seen in Fig.5(d) and Fig.6.

Fundamental wave $\lambda=1.73\mu\text{m}$ is special case when Raman-Nath peaks overlap with Čerenkov. In order to ensure that the process is incoherent for broader spectrum we calculated the angular TH intensity distribution for wavelength range 0.9-2.1 μm . The results are shown in Fig. 11 which depicts the

angular TH intensity distribution for few values of the dispersions of the domain width, $\sigma = 0.05\mu\text{m}$, $\sigma=0.2\mu\text{m}$, $\sigma=1\mu\text{m}$ and $\sigma=10\mu\text{m}$. Maps in the left column (a-d) are obtained assuming incoherent contributions to the total intensity. On the other hand, maps (e-h) represent coherent superposition of constituent harmonic waves (averaged over 45 random samples). It is clear that both models lead to the same emission maps. While of course the actual intensity of the emitted TH signal in incoherent and coherent models will differ, in particular for small dispersion case, the angular dependence of the emitted TH will be the same. Again we clearly see that the out of many discrete TH emission channels clearly visible in ideal periodic structure only the strongest, namely those involving Čerenkov and forward emission are preserved in highly disordered regime.

5 Conclusions

In conclusions, we investigated theoretically the second and third harmonic generation in periodically poled nonlinear crystals with random ferroelectric domain distribution. In particular, we discuss properties of second and cascaded third harmonic generation. We derived analytical formulas describing emission properties of the second and third harmonics in the presence of domain disorder. We showed that in the limit of large number of domains, the THG process is described by product of simple expressions describing each of the constituent processes, i.e. SHG and sum frequency mixing. We considered various processes involved in the frequency mixing and analyzed their properties as a function of wavelength and degree of domain disorder. We show that the randomness-induced incoherence in the wave interaction leads to deterioration and angular spreading of harmonic generated in the processes relying on transverse phase matching such as Raman-Nath. On the other hand forward and Čerenkov frequency generation are basically insensitive to the domain randomness.

This work was supported by the Australian Research Council.

References

1. M. Houe and P. D. Townsend, J. Phys. D: Appl. Phys. **28**, 1747 (1995).
2. J. A. Armstrong, N. Bloembergen, J. Ducuing, and P. S. Pershan, Phys. Rev. **127**, 1918 (1962).
3. P. A. Franken and J. F. Ward, Rev. Mod. Phys. **35**, 23 (1963).
4. M. Fejer, G. Magel, D. Jundt, and R. Byer, IEEE J. Quantum Electron. **28**, 2631 (1992).
5. S. Saltiel, W. Krolikowski, D. Neshev, and Y. S. Kivshar, Opt. Express **15**, 4132 (2007).
6. E. Tal, V.-B. Noa, G.-P. Ayelet, and A. Arie, Nat. Photon. **3**, 395 (2009).
7. S.-n. Zhu, Y.-y. Zhu, and N.-b. Ming, Science **278**, 843 (1997).
8. X. F. C. M. Lu, J. Nonlinear Opt. Phys. Mater. **16**, 185 (2007).
9. U. K. Sapaev and G. Assanto, Opt. Express **16**, 1 (2008).

10. K. Fradkin-Kashi, A. Arie, P. Urenski, and G. Rosenman, *Phys. Rev. Lett.* **88**, 023903 (2001).
11. A. Arie and N. Voloch, *Laser & Photon. Rev.* **4**, 355 (2010).
12. Y. Sheng *et al.*, *Opt. Express* **18**, 16539 (2010).
13. M. Horowitz, A. Bekker, and B. Fischer, *Appl. Phys. Lett.* **62**, 2619 (1993).
14. S. Kawai, T. Ogawa, H. S. Lee, R. C. DeMattei, and R. S. Feigelson, *Appl. Phys. Lett.* **73**, 768 (1998).
15. V. V. Shvartsman, W. Kleemann, T. Łukasiewicz, and J. Dec, *Phys. Rev. B* **77**, 054105 (2008).
16. M. Baudrier-Raybaut, R. Haidar, P. Kupecek, P. Lemasson, and E. Rosencher, *Nature* **432**, 374 (2004).
17. A. Bahabad, O. Cohen, M. M. Murnane, and H. C. Kapteyn, *Opt. Lett.* **33**, 1936 (2008).
18. A. S. Aleksandrovsky, A. M. Vyunishev, A. I. Zaitsev, and V. V. Slabko, *Phys. Rev. A* **82**, 055806 (2010).
19. P. Molina, M. O. Ramirez, and L. E. Bausi, *Adv. Funct. Mat.* **18**, 709 (2008).
20. V. Roppo *et al.*, *Opt. Express* **18**, 4012 (2010).
21. M. Ayoub, J. Imbrock, and C. Denz, *Opt. Express* **19**, 11340 (2011).
22. J. J. Romero, D. Jaque, J. G. Sole, and A. A. Kaminskii, *Appl. Phys. Lett.* **81**, 4106 (2002).
23. J. J. Romero *et al.*, *J. Appl. Phys.* **93**, 3111 (2003).
24. M. Ramirez, J. Romero, P. Molina, and L. Bausi, *Appl. Phys. B* **81**, 827 (2005).
25. A. R. Tunyagi, M. Ulex, and K. Betzler, *Phys. Rev. Lett.* **90**, 243901 (2003).
26. J. Trull *et al.*, *Opt. Express* **15**, 15868 (2007).
27. V. Roppo *et al.*, *Opt. Express* **16**, 14192 (2008).
28. R. Fischer, S. M. Saltiel, D. N. Neshev, W. Krolikowski, and Y. S. Kivshar, *Appl. Phys. Lett.* **89**, 191105 (2006).
29. R. Fischer *et al.*, *Appl. Phys. Lett.* **91**, 031104 (2007).
30. Y. Sheng *et al.*, *Appl. Phys. Lett.* **99**, 031108 (2011).
31. I. Varon, G. Porat, and A. Arie, *Opt. Lett.* **36**, (to be published) (2011).
32. J. S. Pelc, C. Langrock, Q. Zhang, and M. M. Fejer, *Opt. Lett.* **35**, 2804 (2010).
33. J. S. Pelc, C. R. Phillips, D. Chang, C. Langrock, and M. M. Fejer, *Opt. Lett.* **36**, 864 (2011).
34. S. Helmfrid and G. Arvidsson, *J. Opt. Soc. Am. B* **8**, 797 (1991).
35. S. Stivala *et al.*, *Opt. Lett.* **35**, 363 (2010).
36. W. Wang *et al.*, *Opt. Express* **17**, 20117 (2009).
37. Y. Sheng, S. M. Saltiel, and K. Koynov, *Opt. Lett.* **34**, 656 (2009).
38. W. Wang *et al.*, *J. Phys. B* **43**, 215404 (2010).
39. Y. Sheng, W. Wang, K. Kalinowski, K. Koynov, and W. Krolikowski, *Appl. Phys. B-Lasers Opt.* **103**, 13 (2011).
40. S. Russell, P. Powers, M. Missey, and K. Schepler, *IEEE J. Quantum Electron.*, **37**, 877 (2001).
41. Y. L. Grand, D. Rouede, C. Odin, R. Aubry, and S. Mattauch, *Opt. Comm.* **200**, 249 (2001).
42. P. K. Tien, R. Ulrich, and R. J. Martin, *Appl. Phys. Lett.* **17**, 447 (1970).
43. Y. Sheng *et al.*, *Opt. Lett.* **36**, 2593 (2011).
44. S. M. Saltiel *et al.*, *Opt. Lett.* **34**, 848 (2009).
45. Y. Sheng *et al.*, *Opt. Lett.* **36**, 3266 (2011).
46. G. J. Edwards and M. Lawrence, *Opt. Quantum Electron.* **16**, 373 (1984).
47. V. Berger, *Phys. Rev. Lett.* **81**, 4136 (1998).
48. H. Ren, X. Deng, and X. Chen, (2010), arXiv:1010.1593v1.